Lamb wave (A_0 mode) scattering directionality at defects

Paul Fromme

Citation: AIP Conference Proceedings **1806**, 030002 (2017); doi: 10.1063/1.4974570

View online: https://doi.org/10.1063/1.4974570

View Table of Contents: http://aip.scitation.org/toc/apc/1806/1

Published by the American Institute of Physics

Lamb Wave (A_0 Mode) Scattering Directionality at Defects

Paul Fromme

Department of Mechanical Engineering, University College London, WC1E 7JE, UK

p.fromme@ucl.ac.uk

Abstract. Localized and distributed guided ultrasonic waves array systems offer an efficient way for the structural health monitoring of large structures. The detection sensitivity for fatigue cracks depends on the orientation of the crack relative to the location of the sensor elements. Crack-like defects have a directionality pattern of the scattered field depending on the angle of the incident wave relative to the defect orientation and on the ratio of the defect depth and length to the wavelength. From FE simulations it has been shown that for cracks and notches almost no energy is scattered in certain directions from the defect, i.e., the data processing algorithm must take into account that for some transducer combinations no change in the signal even for a significant defect will be detected. The scattered wave field directionality pattern for an incident low frequency A_0 Lamb wave mode was predicted from 3D Finite Element simulations and verified from experimental measurements at machined part-through and through-thickness notches using a laser interferometer. Good agreement was found and the directionality pattern can be predicted accurately. The amplitude of the scattered wave was quantified for a systematic variation of the angle of the incident wave relative to the defect orientation, the defect depth, and the ratio of the characteristic defect size to the wavelength. Based on these results the detection sensitivity for crack-like defects in plate structures using guided wave sensor arrays can be quantified.

INTRODUCTION

The development of fatigue cracks in aircraft structures poses a potential safety risk, necessitating nondestructive testing (NDT) and structural health monitoring (SHM). Guided ultrasonic waves can propagate over long distances in structures that are thin in at least one dimension, providing an efficient way for the SHM of large structures [1, 2]. High frequency guided waves have been employed to monitor fatigue crack growth at fastener holes [3-6] and to detect defects in multi-layered structures [7]. For plate structures, localized and distributed array systems using low-frequency guided ultrasonic waves have been developed for the detection of defects [8-11]. Taking the scattering pattern into account for the signal processing, e.g. minimum variance imaging for distributed sensors, has been shown to improve the sensitivity for crack-like defects and to allow for the estimation of the defect orientation [12].

The scattering of the A_0 Lamb wave mode at a through thickness hole [13], part thickness hole [14], 2D notch [15] and fatigue crack emanating from a fastener hole has been reported previously [16]. Continuing from previous contributions [17-19], the directionality pattern of the A_0 Lamb wave mode scattered at crack-like defects (notch) in a plate is investigated, depending on the angle of the incident wave relative to the crack orientation and on the defect length relative to the wavelength. The scattered wave fields predicted from Finite Element (FE) simulations and measured experimentally are compared and show good agreement for part-through and through thickness notches of different length. The obtained scattering characteristics are discussed with a view towards the detection of crack-like defects using guided ultrasonic waves.

43rd Annual Review of Progress in Quantitative Nondestructive Evaluation, Volume 36
AIP Conf. Proc. 1806, 030002-1–030002-9; doi: 10.1063/1.4974570
Published by AIP Publishing. 978-0-7354-1474-7/$30.00

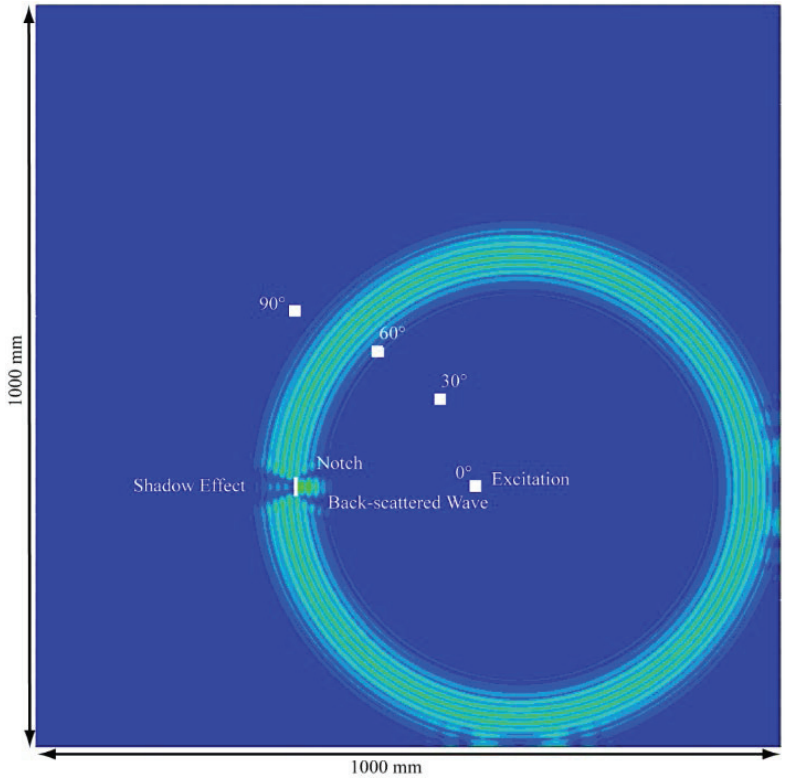

FIGURE 1. Time snapshot of FE plate simulation, top view; f = 100 kHz; λ = 19 mm; a = 20 mm; through thickness notch and excitation locations at 0°, 30°, 60°, and 90° shown; wave crest propagating radially outwards from 0° excitation point, wave scattered at notch with shadow effect and back-scattered wave visible.

FINITE ELEMENT SIMULATION

The scattering of the first anti-symmetric A_0 Lamb wave mode was simulated using three-dimensional (3D) Finite Element (FE) models with linear brick elements in ABAQUS Explicit. The model of a 5 mm thick aluminum plate (size: 1 m x 1 m) with a notch of varying length and depth was implemented, similar to the model described in [20]. The notch was modeled by removing one row of the brick elements to achieve the desired length and depth. Explicit time integration was used, and the element size and time step were chosen to adhere to the usual stability criteria. Point excitation of the A_0 Lamb wave mode was introduced at chosen node locations 300 mm from the defect location, allowing for a variation of the incidence angle between 0° and 90°, relative to the normal of the notch. The excitation pulse was set as a 5 cycle toneburst with a center frequency of 100 kHz, giving a wavelength λ for the A_0 mode of 19 mm. The amplitude of the A_0 mode was recorded as the out-of-plane displacement at the center (mid-plane) node on points in a square area around the defect. The time trace at each monitoring node was time gated to remove reflections from the plate edges. Fast Fourier Transform (FFT) was used to extract the complex magnitude (amplitude and phase information) at the center frequency of 100 kHz for each monitoring node. This captures the combined wave field of the incident wave and scattered wave. Additional simulations were run to capture the incident wave field only, without a defect present. Taking the difference between the complex magnitudes for each point with and without a defect, the amplitude of the wave scattered at the defect can be isolated [13]. The amplitude of the scattered wave was extracted on a radius of 30 mm by interpolating between monitoring nodes to obtain an amplitude value every 5 degree. The methodology is described in more detail in previous contributions [17, 19].

EXPERIMENTS

The scattered wave field around a 5 mm and a 20 mm long notch was measured on a large, 5mm thick aluminum plate (size: 1.5 m x 1 m). The notches (width: 1 mm) were milled in four steps to give a varying depth of ¼, ½, ¾, and through thickness. The notch had rounded edges due to the milling tool (diameter 1 mm) and a flat bottom for the part-through depths. Three excitation transducers were placed 300 mm away from the center of the notch location to

give angles of the incident wave of 0°, 45° and 90° relative to the normal of the notch (Fig. 2). The transducers consist of a PZT disc (Ferroperm Pz27, diameter 5 mm, thickness 2 mm) and a brass backing mass (height 6 mm) and were permanently bonded to the plate using two-component epoxy glue. The transducers act in good approximation as point sources for the excitation of the first antisymmetric Lamb wave mode A_0.

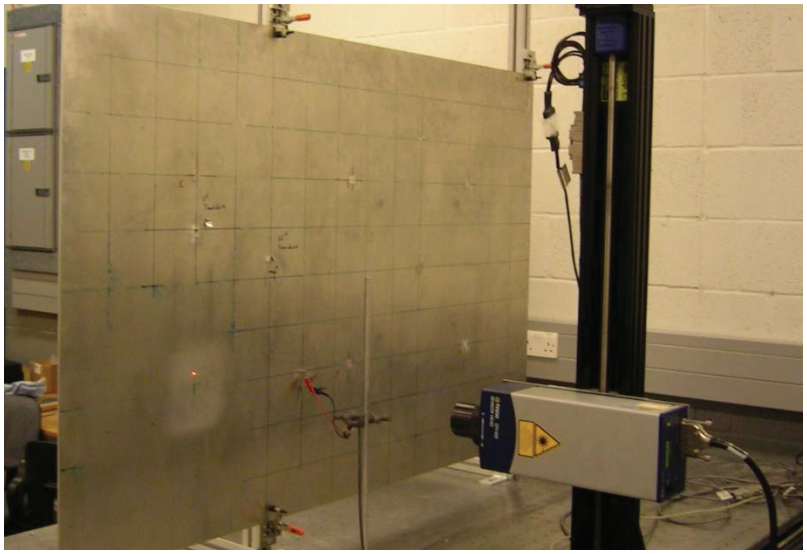

FIGURE 2. View of experimental setup: aluminum plate (size: 1.5 m x 1 m) with 20 mm notch, 3 excitation transducers at 0°, 45°, and 90°, 300 mm from notch, and laser interferometer.

The excitation signal was a 5 cycle toneburst with a center frequency of 100 kHz modulated by a Hanning window. The signal was generated in a programmable function generator and amplified using a power amplifier. The velocity of the out-of-plane displacement was measured using a laser interferometer every 5 degrees on a circle around the notch with a radius of 30 mm. The full time traces of the measured signals were bandpass filtered (75 kHz – 125 kHz) and averaged in a digital oscilloscope before being transferred to the measurement PC [13]. Similar to the FE simulations, an initial measurement was done for each excitation transducer before the milling of the notch to capture the incident wave field, and then for each notch depth. The measured time traces were time gated and the amplitude and phase (complex magnitude) at 100 kHz determined using FFT. Due to the re-positioning of the plate after each milling step relative to the laser, the repeatability of the phase measurement was not perfect. This leads to a noise level of about 5% of the amplitude of the incident wave when taking the difference between complex magnitudes to evaluate the scattered field. The amplitudes were normalized with the amplitude of the incident wave.

SCATTERING PATTERN COMPARISON

Shown in Fig. 3 are the polar plots of the measured and simulated amplitude patterns for the wave scattered at a 20 mm long defect (approximately λ) for an incident wave from the 0° direction (perpendicular to the defect orientation). For this incident wave direction the scattering pattern is symmetric, with a back-scattered lobe in the 0° direction and a shadow area in the 180° direction, where the defect blocks the incident wave path and amplitude reduction occurs. From the scattering patterns it is clear that almost no scattering occurs along the defect orientation, i.e., in the 90° and 270° directions. For a shallow defect (1/4 depth, Fig. 3a) the amplitude of both the back and forward scattered wave lobes are rather small. As the repositioning of the plate for the measurements leads to an error in the scattered wave amplitude calculation of about 5% of the incident wave, an irregular pattern for the experimental curve can be observed. With increasing defect depth initially the amplitude of the forward scattered lobe (shadow area) increases and an increased backscattered wave is observed for a deep (through thickness, Fig. 3d) defect. Good agreement of the measured and simulated amplitude patterns can be observed, helping to validate the FE simulations. For an incident wave at a 45° angle to the defect orientation (20 mm length) again good agreement of the wave patterns can be observed in Fig. 4. For shallow defects mostly a blocking of the forward wave path with a reduced amplitude around the 225° direction can be observed. Only for a through thickness defect a specular scattering pattern (angle of reflected wave equals angle of incident wave) can be observed in Fig. 4d.

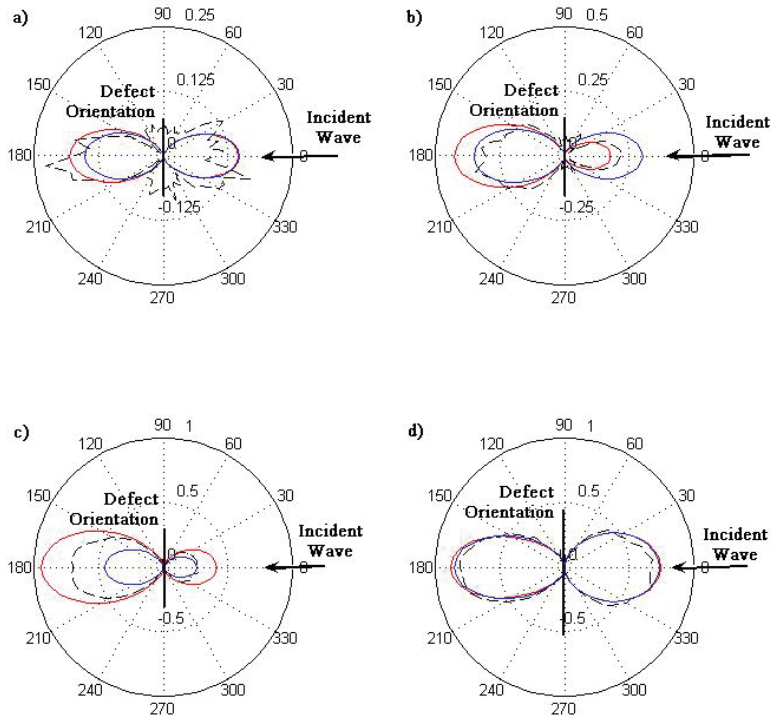

FIGURE 3. Polar plot of normalized amplitude of A_0 mode scattered at defect (monitored at 30 mm radius); orientation 90°-270°; incident wave from 0°; f = 100 kHz; λ = 19 mm; a = 20 mm; experiment notch (black, dashed), simulation notch (red, solid), simulation crack (blue, solid): a) ¼ thickness; b) ½ thickness; c) ¾ thickness; d) through thickness.

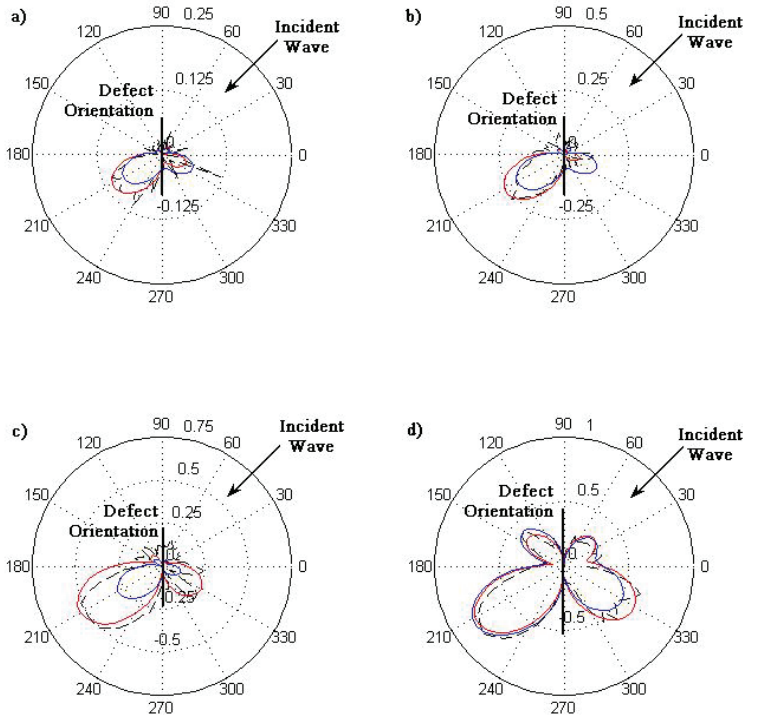

FIGURE 4. Polar plot of normalized amplitude of A_0 mode scattered at defect (monitored at 30 mm radius); orientation 90°-270°; incident wave from 45°; f = 100 kHz; λ = 19 mm; a = 20 mm; experiment notch (black, dashed), simulation notch (red, solid), simulation crack (blue, solid): a) ¼ thickness; b) ½ thickness; c) ¾ thickness; d) through thickness.

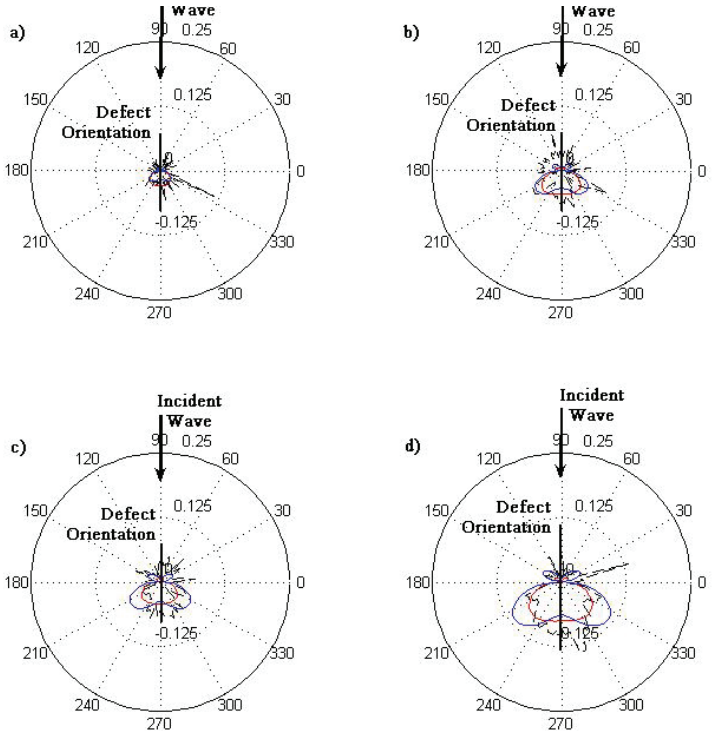

FIGURE 5. Polar plot of normalized amplitude of A_0 mode scattered at defect (monitored at 30 mm radius); orientation 90°-270°; incident wave from 90°; f = 100 kHz; λ = 19 mm; a = 20 mm; experiment notch (black, dashed), simulation notch (red, solid), simulation crack (blue, solid): a) ¼ thickness; b) ½ thickness; c) ¾ thickness; d) through thickness.

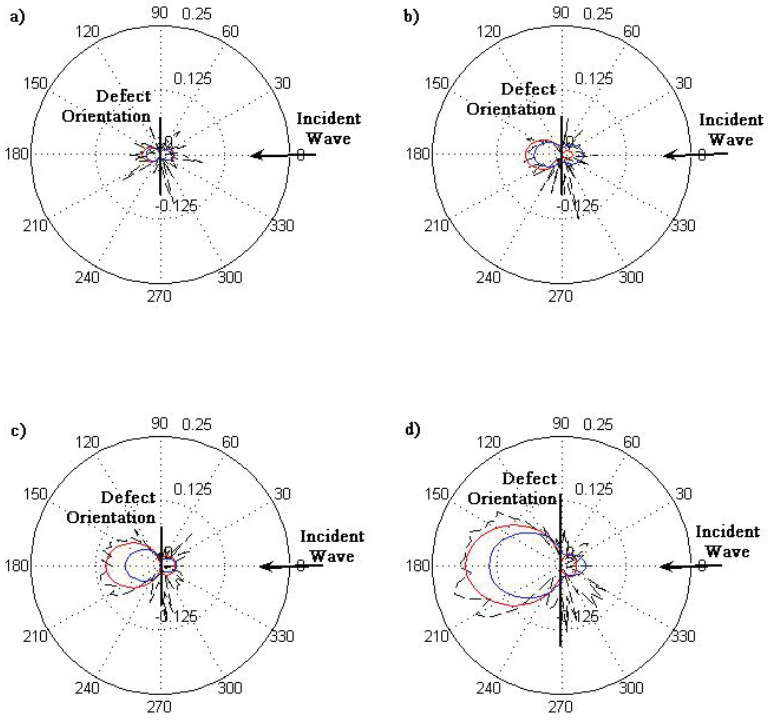

FIGURE 6. Polar plot of normalized amplitude of A_0 mode scattered at defect (monitored at 30 mm radius); orientation 90°-270°; incident wave from 0°; f = 100 kHz; λ = 19 mm; a = 5 mm; experiment notch (black, dashed), simulation notch (red, solid), simulation crack (blue, solid): a) ¼ thickness; b) ½ thickness; c) ¾ thickness; d) through thickness.

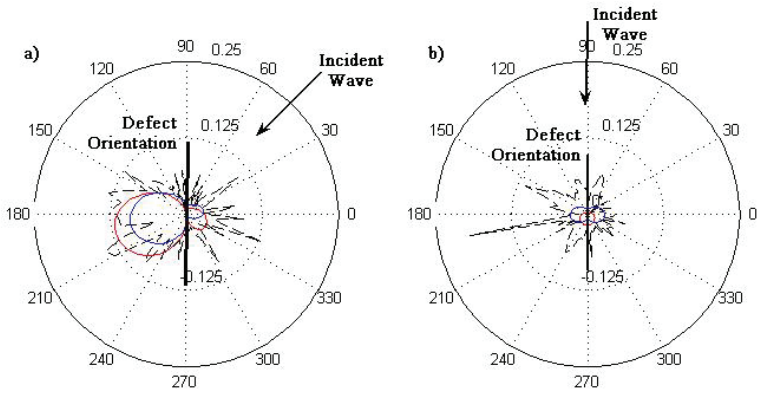

FIGURE 7. Polar plot of normalized amplitude of A_0 mode scattered at defect (monitored at 30 mm radius); orientation 90°-270°; through thickness; f = 100 kHz; λ = 19 mm; a = 5 mm; experiment notch (black, dashed), simulation notch (red, solid), simulation crack (blue, solid): a) incident wave from 45°; b) incident wave from 90°.

For the case of the incident wave propagating along the defect orientation (90° incident wave direction) shown in Fig. 5 only very limited scattering occurs. For shallow defects the predicted scattered wave amplitude is very low and due the experimental noise it is not possible to measure it accurately. For deep defects the simulations predict a scattered wave amplitude of about 10% of the incident wave and a reasonable good agreement between measurements and predictions can be seen in Fig. 5d.

Measurements and simulations were then done for the case of a short defect (5 mm length), with a length of about $\lambda/4$ to investigate the limitations for defect detection. For the case of a shallow (1/4 depth) defect with an incident wave from the 0° direction, the predicted scattered amplitude is very small and no experimental scattering can be observed in Fig. 6a. With increasing defect depth a forward scattered wave can be seen, with good agreement between measurements and simulations. In contrast to the previous results for a long defect, only a forward scattered wave due to the blocking of the wave path can be seen in Fig. 6, with very limited scattered amplitude in all other directions, including the backscattered direction (0°). For the other incident wave directions the scattered wave amplitude was small and only the case of a through thickness defect is shown in Fig. 7. For an incident wave from the 45° direction a small forward scattered wave can be observed in Fig. 7a, but for an incident wave propagating along the defect orientation (90° incident wave direction) almost no scattering is predicted and measured (Fig. 7b).

From this comparison the FE simulations could be validated and certain patterns could be observed, which should be taken into account for the prediction of defect detection sensitivity using guided wave arrays [20]. Almost no scattered wave was observed along the defect orientation and for an incident wave propagating along this direction. For shallow and short defects mostly a shadow area behind the defect with reduced amplitude due to the blocking of the wave path (shadow area) was found. Large backscattered wave amplitude or a specular scattering pattern were mostly observed for defects that are deep and long compared to the wavelength of the incident wave.

SCATTERING PATTERN PREDICTION

The FE simulations were used to predict the scattering patterns and amplitudes for a variation of the geometrical parameters over a wide range. Figure 8 shows the predicted maximum scattered amplitude for a variation of the incident wave direction relative to the defect orientation. For the case of a short (5 mm length), through thickness defect (Fig. 8a) it can be observed that the amplitude decreases as the incident wave direction changes from 0° (perpendicular) to 90° (along defect). Only small scattered wave amplitude is predicted for the 90° incident wave direction and such a defect would be very difficult to detect experimentally. For the case of a long (20 mm length), through thickness defect significantly higher amplitudes are predicted and such a defect could be detected for most incident wave directions (Fig. 8b). The simulations show the highest scattered wave amplitude not for the case of the perpendicular incident wave, but at a slight angle, which should be investigated further.

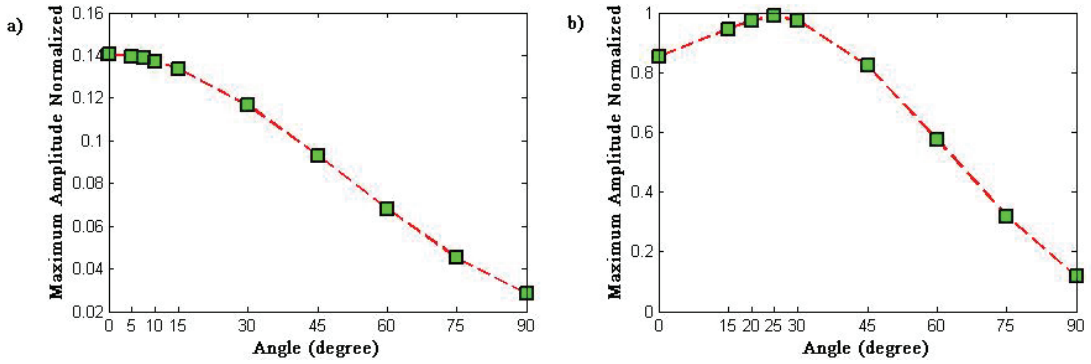

FIGURE 8. Maximum scattered amplitude of A_0 mode (monitored at 30 mm radius) for variation of incident wave direction (perpendicular: 0°, along defect: 90°); through thickness; f = 100 kHz; λ = 19 mm, defect length: a) 5 mm; b) 20 mm.

Figure 9 shows the predicted maximum scattered wave amplitude from the FE simulations for the cases of a through thickness and half thickness defect with increasing length and two incident wave directions. For the case of a through thickness defect (Fig. 9a/b) the amplitude increases with defect length and significant scattered waves with similar amplitudes to the incident wave are predicted. However, it should be noted that the maximum scattered amplitude does not increase linearly with length, but that a stepped pattern, especially for the 45° incident wave direction (Fig. 9b) can be observed. This occurs at approximately half wavelength (10 mm defect length) and wavelength and correlates to observed changes in the angular scattering pattern. For the case of a defect half through the plate thickness, lower scattered amplitude but a mostly linear increase with defect length can be seen in Fig. 9c/d. Low scattered amplitude for short, part-thickness defects would make long-range detection difficult, but for longer defects scattered amplitudes comparable to approximately half the incident wave amplitude are predicted.

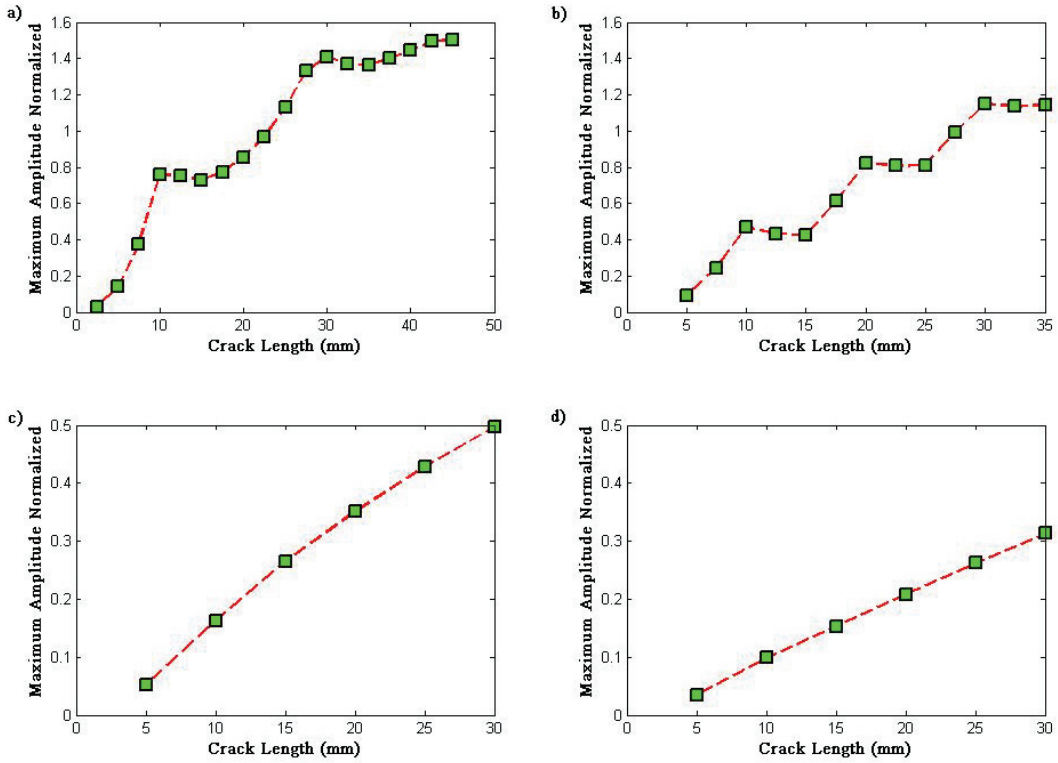

FIGURE 9. Maximum scattered amplitude of A_0 mode (monitored at 30 mm radius) for variation of defect length; f = 100 kHz; λ = 19 mm: a) defect through thickness, incident wave from 0° direction (perpendicular); b) defect through thickness, incident wave from 45° direction; c) defect half thickness, incident wave from 0° direction (perpendicular); d) defect half thickness, incident wave from 45° direction.

CONCLUSIONS

The scattering of the first anti-symmetric guided wave mode in isotropic plates (A_0 Lamb mode) at part-through and through thickness crack-like defects has been measured experimentally and predicted from FE simulations. Reasonably good agreement was found between the FE predicted and experimentally measured scattered field directivity patterns and amplitudes. This allows for the further investigation of the influence of defect size and incident wave angle from FE simulations. For small scattered amplitudes the sensitivity of the measurements is slightly limited due to the requirement of a baseline subtraction to isolate the scattered wave from the incident wave. Almost no scattered wave was observed along the defect orientation and for an incident wave propagating along this direction. For shallow and short defects mostly a shadow area behind the defect with reduced amplitude due to the blocking of the wave path (shadow area) was found. Large backscattered wave amplitude or a specular scattering pattern were mostly observed for defects that are deep and long compared to the wavelength of the incident wave. The FE simulations predict a significant increase in the scattered wave amplitude for long defects and for the case of the incident wave mostly perpendicular to the defect orientation. These results can be beneficial for the development of permanently attached guided wave arrays for SHM. Predicted scattering patterns can be taken into account for the signal processing, e.g. minimum variance imaging, and the sensitivity for crack-like defects improved compared to a standard delay and sum approach. As the sensitivity for defect detection will depend strongly on the location of the sensors relative to the defect locations, improved configurations for distributed sensor array systems can be proposed and the sensitivity for the detection of defects at likely locations and orientations can be quantified and predicted.

ACKNOWLEDGMENTS

The author would like to thank Clemence Rouge for her contributions to the measurements and the simulations.

REFERENCES

1. J.L. Rose, *Mat. Eval.* **60**, 53-59 (2002).
2. Z. Fan, M. Castaings, M.J.S. Lowe, C. Biateau, and P. Fromme, *NDT&E Int.* **54**, 96-102 (2013).
3. B. Masserey and P. Fromme, "In-situ Monitoring of Fatigue Crack Growth at Fastener Holes Using Rayleigh-like Waves," in *Review of Progress in Quantitative Nondestructive Evaluation*, eds. D.O. Thompson and D.E. Chimenti, (AIP Conf. Proc. 975, New York) **27**, 1484-1491 (2008).
4. B. Masserey and P. Fromme, *Struct. Health Monit.* **12**, 484-493 (2013).
5. B. Masserey and P. Fromme, *NDT&E Int.* **71**, 1-7 (2015).
6. H. Chan, B. Masserey, and P. Fromme, *Smart Mater. Struct.* **24**, 025037 (2015).
7. B. Masserey, C. Raemy, and P. Fromme, *Ultrasonics* **54**, 1720-1728 (2014).
8. P. Fromme, P. D. Wilcox, M.J.S. Lowe, and P. Cawley, *IEEE Trans. Ultrason. Ferroelectr. Freq. Control* **53**, 777-785 (2006).
9. A.J. Croxford, P.D. Wilcox, B.W. Drinkwater, and G. Konstantinidis, *Proc. Roy. Soc. A*, **463**, 2961-2981 (2007).
10. J.E. Michaels and T.E. Michaels, *Wave Motion* **44**, 482-492 (2007).
11. P. Fromme, "Monitoring of Plate Structures Using Guided Ultrasonic Waves," in *Review of Progress in Quantitative Nondestructive Evaluation*, ed. by D.O. Thompson and D.E. Chimenti, (American Institute of Physics 975, Melville, NY), **27**, 78-85 (2008).
12. J.S. Hall, P. Fromme, and J.E. Michaels, *J. Nondestruct. Eval.* **33**, 299-308 (2014).
13. P. Fromme and M.B. Sayir, *J. Acoust. Soc. Am.* **111**, 1165-1170 (2002).
14. P. Fromme, P.D. Wilcox, M. Lowe, and P. Cawley, "On the Scattering and Mode Conversion of the A_0 Lamb Wave Mode at Circular Defects in Plates," in *Review of Progress in Quantitative Nondestructive Evaluation*, eds. D.O. Thompson and D.E. Chimenti, (American Institute of Physics 700, Melville, NY) **23**, 142-149 (2004).
15. M.J.S. Lowe, P. Cawley, J.Y. Kao, O. Diligent, *J. Acoust. Soc. Am.* **112**, 2612-2622 (2002).
16. P. Fromme and M. B. Sayir, *Ultrasonics* **40**, 199-203 (2002).
17. C. Rouge and P. Fromme, "Directivity of guided ultrasonic wave scattering at notches and cracks," *J. Phys.: Conf. Ser.* **269**, 012018 (2011).
18. P. Fromme, "SHM of large structures using guided waves for crack detection," in *Review of Progress in Quantitative Nondestructive Evaluation*, eds. D.O. Thompson and D.E. Chimenti, (American Institute of Physics 1335, Melville, NY) **30**, 1507-1514 (2011).

19. P. Fromme, "Directionality of the scattering of the A0 Lamb wave mode at cracks," in *Review of Progress in Quantitative Nondestructive Evaluation*, ed. by D.O. Thompson and D.E. Chimenti, (American Institute of Physics 1211, Melville, NY) **29**, 129-136 (2010).
20. P. Fromme, "Health Monitoring of Plate Structures using Guided Waves," *Proc. SPIE* **6935**, 69350W (2008).